2019 International Conference on Robotics and Automation (ICRA)
Palais des congres de Montreal, Montreal, Canada, May 20-24, 2019

Integrated UWB-Vision Approach for Autonomous Docking of UAVs in GPS-denied Environments

Thien-Minh Nguyen*, Thien Hoang Nguyen*, Muqing Cao*, Zhirong Qiu*, Lihua Xie*, *Fellow, IEEE*

***Abstract*— Though vision-based techniques have become quite popular for autonomous docking of Unmanned Aerial Vehicles (UAVs), due to limited field of view (FOV), the UAV must rely on other methods to detect and approach the target before vision can be used. In this paper we propose a method combining Ultra-wideband (UWB) ranging sensor with vision-based techniques to achieve both autonomous approaching and landing capabilities in GPS-denied environments. In the approaching phase, a robust and efficient recursive least-square optimization algorithm is proposed to estimate the position of the UAV relative to the target by using the distance and relative displacement measurements. Using this estimate, UAV is able to approach the target until the landing pad is detected by an onboard vision system, then UWB measurements and vision-derived poses are fused with onboard sensor of UAV to facilitate an accurate landing maneuver. Real-world experiments are conducted to demonstrate the efficiency of our method.**

I. Introduction

Autonomous docking of Unmanned Aerial Vehicles (UAVs) has been an active research area over the past decade. In general, it consists of two phases: an approaching phase and a landing phase. Firstly, the UAV needs to locate and navigate towards the target, which can be a landing track, a manned or unmanned ground vehicle, possibly from some distance up to a hundred meters away. Once the UAV is in close proximity of the target, it will try to land in a predefined area. Conventionally, onboard vision systems are widely employed to perform precise landing [1]–[8] due to their ability to provide accurate positioning information. However, while the landing problem can be considered mature by the use of vision, it comes to our attention that the approaching problem still lacks a good solution.

In many cases when GPS is available, the approaching capability can be achieved by simply communicating GPS data between the UAV and the target. Recent works have showed that by integrating GPS and vision data, the UAV can land on a vehicle moving at 50 km/h [9], or a fixed-wing UAV can successfully dock onto a mid-air target [10]. However, this method depends greatly on the availability and the quality of GPS signals, and hence can only be applied in limited scenarios. Specifically, it cannot be applied in city canyons, forests, caves, or deep mines. Other methods have also been proposed under GPS-denied conditions. For example, Kong et. al. [11] proposed a method using a ground based stereo camera to track and guide the UAV in the landing process. Similarly, Gui et. al. [12] reversed the solution by having the UAV carry the camera to detect infrared signals from special lamps installed at the destination. It should be noted that these works are only concerned with landing the UAV on a static target, which require a long calibration process and can be easily affected by background lighting conditions. Also they do not entirely resolve the issue when the target is out of the view of the UAV, or vice versa.

In this work, we consider the autonomous docking problem of UAVs onto a moving Unmanned Ground Vehicle (UGV) from a long distance, by integrating Ultra-Wide Band (UWB) and vision sensors to provide accurate and reliable relative localization. Due to its omni-directional sensing capability and strong resistance to multipath and other inferences, UWB sensors are able to obtain high ranging accuracy over long operation range (an error up to 10cm with maximum range up to 50 m is typical for the sensor used in our case[1]), not to mention its communication functionality. In our work, a set of UWB nodes are installed on the UGV and the UAV, serving to measure the relative distance and exchange information. In addition, both vehicles are equipped with high-accuracy visual odometry systems [13], [14] to collect displacement measurements, which are transmitted through UWB message. By combining the distance and displacement measurements, we propose a relative localization scheme based on recursive least square optimization, and rigorously prove the exponential convergence to the true relative position. Based on this relative position estimate, the UAV is able to fulfill the approaching and landing tasks from an initial large distance relative to the target. Extensive outdoor flight tests have been conducted to demonstrate that the UAV can approach the moving UGV from 50m away and then accurately land on a 1.5m×2m large platform.

In summary, the main contributions of our work can be specified as follows:

- We design a relative localization scheme by using distance measurements from sequential ranging to UWB anchors and relative displacement measurements from visual odometers. We then propose a recursive least square algorithm to estimate the relative position to the moving target, and show that the estimation error converges to zero exponentially fast.
- Compared with our previous works on distance-based docking with static targets [15]–[17], this work focuses

The authors are with School of Electrical and Electronic Engineering, Nanyang Technological University, Singapore 639798, 50 Nanyang Avenue.
∗ These authors contributed equally to the work.
⋆ Corresponding author: elhxie@e.ntu.edu.sg

A video summarizing the main concepts and experiment results of this paper can be downloaded as supplementary media materials on http://ieeexplore.ieee.org, or viewed directly at https://youtu.be/qvDkEuIzzYs.

[1] http://www.timedomain.com/products/pulson-440/

978-1-5386-6027-0/19/$31.00 ©2019 IEEE

on the cooperative docking of a UAV on a moving target, which achieves much higher flexibility for the docking task. Moreover, in those works no exponential convergence was achieved.

- In the landing phase, we propose a method to fuse both relative position estimate and range measurement to ensure an accurate landing maneuver on a small moving platform. We have conducted extensive indoor and outdoor experiments to show the efficacy and efficiency of the integrated UWB-vision approach from a distance up to 50m.

The remaining of this paper is organized as follows: In Section II, we describe the key definitions and an overview of the integrated UWB-vision approach to solve the autonomous docking problem with two specialized estimation-control schemes for approaching and landing tasks. In Section III, we present the relative localization scheme in details along with a proof on its exponential convergence. Section IV presents the results of our real flight experiments with the algorithm implemented in an autonomous docking scenario. Finally, Section V concludes the paper.

II. Overview

A. Basic Definitions

In this section we will define some basic concepts needed for later parts in direct reference to Fig. 1. First, we define p_k as the UAV position relative to the target with respect to an inertial frame of reference F_W. In this work we assume that F_W is aligned with the earth's magnetic field.

In our setup, multiple UWB nodes $a_0, a_1, \ldots, a_{N-1}$ (which also denote their coordinates in the mobile frame F_M fixed on the UGV) are installed on the UGV and another UWB node is also installed on the UAV. Henceforth, we refer to the UWB nodes on the target as the anchors. Note that the UAV node can only range to one anchor at a time and the ranging scheme is executed in a periodic manner as $0, 1, \ldots, N-1, 0, 1 \ldots$ Henceforth, we will also use a_k to denote the coordinates of the anchor a_i that is ranged to at the time step k, where explicit specification of index i is glossed over to keep the notation simple (this detail is not used in subsequent analysis). However, when needed, it can be retrieved by the modulo operation $i = \mod(k, N)$.

As illustrated in Fig. 1, at time $k\tau$ with τ being the sampling time, the following measurements can be obtained: for the UAV, it can measure the distance d_k to only one of the UWB nodes on the UGV, and its own displacement vector ϕ_k^m since the last time step $k-1$ from a visual odometer; for the UGV, it can measure its displacement vector ϕ_k^M and the orientation R_k^M with respect to F_W using its own visual inertial odometry system, and send them to the UAV.

In reference to Fig. 1, we also define $u_k^m = \frac{1}{\tau}\phi_k^m$, $u_k^M = \frac{1}{\tau}\phi_k^M$ as average velocity of the UAV and the UGV respectively from time steps $k-1$ and k. Similarly, we treat the change from R_{k-1}^M to R_k^M as a rotation around an axis e_k from time steps $k-1$ to k with an average angular rate ω_k, as illustrated in Fig. 2.

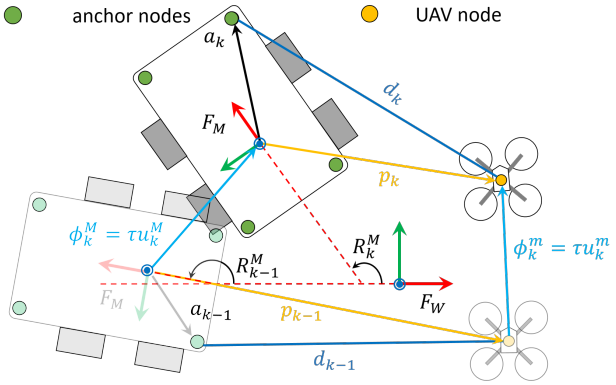

Fig. 1. Visualization of the main concepts defined in Section II-A.

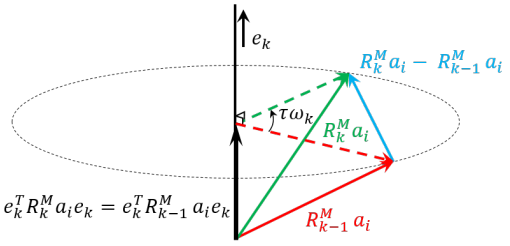

Fig. 2. Characterization of the rotation rate: between two time steps, the frame F_M rotates by an angle $\tau\omega_k$ around the axis e_k. For a vector a_i that is fixed in F_M, its coordinates in the inertial frame F_W at time steps $k-1$ and k will be $R_{k-1}^M a_i$ and $R_k^M a_i$, respectively. It can be seen that $\left\| R_k^M a_i - R_{k-1}^M a_i \right\| \leq 2\|a_i\| \left|\sin(\tau\omega_k/2)\right| \leq \tau \|a_i\| \left|\omega_k\right|$. The equality occurs when a_i is orthogonal to e_k.

B. Estimation-Control Schemes

1) Approaching: In this section we will describe the main ideas for accomplishing the approaching task in direct reference to Fig. 3.

Firstly, the UAV will rely on an optical flow as the main feedback for stable flight control. Note that this optical flow measurement is fused with IMU and other onboard measurements in an *onboard estimator* based on Extended Kalman Filter to obtain the displacement measurement ϕ_k^m.

Secondly, the target's orientation R_k^M and displacement measurement ϕ_k^M (which is obtained from some navigation system mounted on the target, e.g SLAM or visual-inertial odometry) will be sent to the UAV via the same UWB ranging message.

Finally, with the information d_k, a_k, ϕ_k^m, ϕ_k^M, R_k^M, a recursive least square optimization algorithm will be employed to provide an estimate $\hat{p}_k$ of the relative position p_k. Based on this estimate, a velocity command v_k is calculated and sent to the onboard flight controller to drive the UAV towards the target. Specifically, v_k is generated by the following simple negative feedback control rule with saturation:

$$v_k = \bar{v} / \max\{\bar{v}, K_p \|\hat{p}_k\|\}(-K_p \hat{p}_k), \tag{1}$$

where $\bar{v} > 0$ is the maximum desired velocity and $K_p > 0$ is a constant gain.

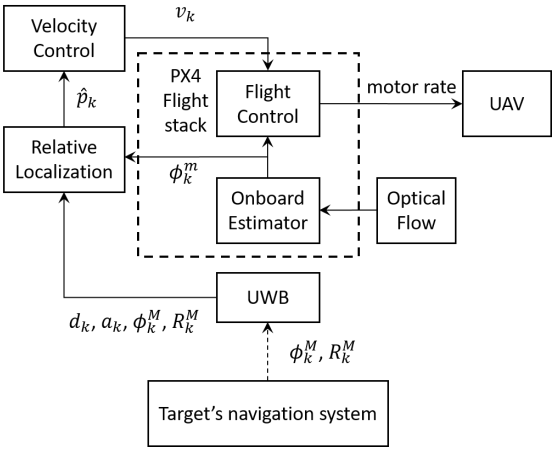

Fig. 3. The estimation-control scheme in the approaching phase. See Section II-B.1 for more details.

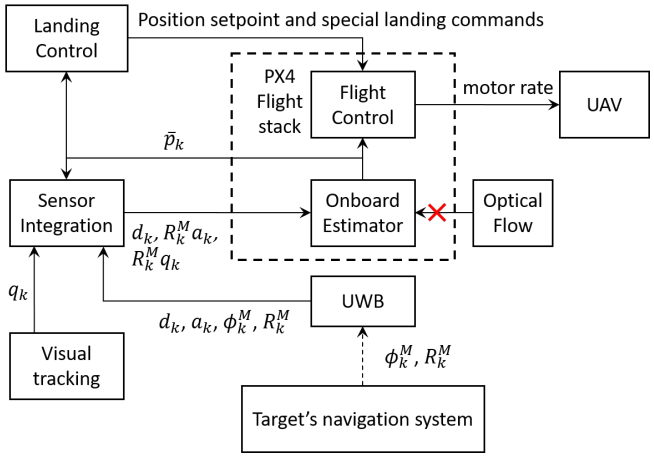

Fig. 4. The estimation-control scheme in the landing phase. See Section II-B.2 for more details.

2) Landing: As the UAV approaches the platform and the optical flow may become unreliable (we found that normal asphalt surface yields more accurate displacement measurement than the landing pad's black and white surface), we will switch to a different estimate-control scheme for more efficient and accurate landing. Specifically, upon the first detection of the visual marker, we will transition to the landing phase where optical flow data is disabled, then both vision and UWB measurements are fused with IMU data in the onboard estimator to facilitate a position-based control rule, which is detailed below.

As seen from Fig. 4, we use the position q_k of the UAV with respect to the target's body frame F_M as the new source of feedback in place of the optical flow. After retrieving q_k from visual tracking information, we can obtain $R_k^M q_k$ as an observation of the relative position p_k, and fuse it into the onboard estimator to generate the relative position estimate $\bar{p}_k$. Moreover, to make up for temporary losses of vision, we also fuse distance measurement into the onboard estimator by invoking the observation model $d_k = \left\|\bar{p}_k - R_k^M a_k\right\|$ in the same manner with the EKF-based fusion scheme in [18].

Finally, using the onboard estimator estimate $\bar{p}_k$ of the relative position p_k, the flight control unit can drive the UAV to the center of the target. We impose that the UAV will only descend when $\bar{p}_k$ is within a proximity of the center and automatically cut off the throttle when the altitude is bellow a threshold.

III. Relative Localization Algorithm

In this section we will discuss the derivation of the recursive least-square estimation algorithm along with the theoretical analysis of the convergence.

First, some standard assumptions will be stated.

A. Assumptions

To ensure a unique solution for later cost function, it is necessary that there are sufficient anchors whose coordinates are linearly independent. In other words, the anchors must not be co-linear in 2D case, or co-planar in 3D case, which is more formally stated as follows:

Assumption 1. *For $p_k \in \mathbb{R}^n$, $n \in \{2, 3\}$, there exist $k_1, \ldots k_n \in \{1, 2, \ldots N\}$ such that* $\text{rank}[b_{k_1} \ldots\ b_{k_n}] = n$, *where $b_{k_i} \triangleq a_{k_i} - a_{k_i - 1}$ and $a_N \equiv a_0$.*

Since both UAV and UGV are physical systems, we also assume that the average relative velocity $u_k = u_k^m - u_k^M$ and the target's rotation rate ω_k are all bounded (indeed, these constraints can also be enforced via some control law with saturation as in (1)):

Assumption 2. *There exist positive constants U and Ω such that $\|u_k\| \leq U$ and $|\omega_k| \leq \Omega$ for all k.*

B. Parametric model

Notations: in this section we will denote R_k^M as R_k to simplify the notation. Also, for a vector v, v' denotes its transpose and $\|v\|$ denotes its Euclidean norm.

By recalling the definitions defined in Section II-A and Fig. 1, we can verify the following relationship between p_k and the measurements d_k, τ, u_k, R_k and a_k:

$$d_k^2 = (p_{k-1} + \tau u_k - R_k a_k)'(p_{k-1} + \tau u_k - R_k a_k), \quad (2)$$

$$d_{k-1}^2 = (p_{k-1} - R_{k-1} a_{k-1})'(p_{k-1} - R_{k-1} a_{k-1}). \quad (3)$$

Noticing that $R_k' R_k = I$, one can expand the right hand side of the previous equations and obtain the following

$$d_k^2 - d_{k-1}^2 = \tau^2 \|u_k\|^2 + \|a_k\|^2 - \|a_{k-1}\|^2 - 2\tau u_k' R_k a_k + 2(\tau u_k - R_k a_k + R_{k-1} a_{k-1})' p_{k-1}. \quad (4)$$

From this relationship, denote the following quantities

$$\zeta_k = \frac{1}{2}\Big(d_k^2 - d_{k-1}^2 - \tau^2 \|u_k\|^2 - \|a_k\|^2 + \|a_{k-1}\|^2 + 2\tau u_k' R_k a_k\Big), \quad (5)$$

$$\varphi_k = \tau u_k - R_k a_k + R_{k-1} a_{k-1}. \quad (6)$$

Thus, by comparing (4), (5), and (6) we can obtain

$$\zeta_k = \varphi_k' p_{k-1}. \quad (7)$$

C. Cost function and estimation update law

With the parametric model (7), let us define $\hat{p}_k$ as the estimate of p_k that minimizes the following cost function:

$$J_k = \frac{1}{2}\sum_{i=1}^{k}\beta^{k-i}(\zeta_i - \varphi_i'(\hat{p}_k - \sum_{j=i}^{k}\tau u_j))^2 + \frac{1}{2}\beta^k(\hat{p}_k - \sum_{j=1}^{k}\tau u_j - \hat{p}_0)'\Gamma_0^{-1}(\hat{p}_k - \sum_{j=1}^{k}\tau u_j - \hat{p}_0), \tag{8}$$

where $\hat{p}_0$ is the initial value of $\hat{p}_k$, Γ_0 is a positive definite matrix, and β is a positive constant.

By solving $\partial J_k/\partial \hat{p}_k = 0$, we obtain the estimator of $\hat{p}_k$ as follows:

$$\epsilon_k = \zeta_k - \varphi_k'\hat{p}_{k-1}, \tag{9a}$$

$$\Gamma_k = \frac{1}{\beta}\left(\Gamma_{k-1} - \frac{\Gamma_{k-1}\varphi_k\varphi_k'\Gamma_{k-1}}{\beta + \varphi_k'\Gamma_{k-1}\varphi_k}\right), \tag{9b}$$

$$\hat{p}_k = \hat{p}_{k-1} + \tau u_k + \Gamma_k\varphi_k\epsilon_k, \tag{9c}$$

where $0 < \beta < 1$, $\Gamma_k \in \mathbb{R}^{n\times n}$ and $\Gamma_0 = \gamma I$ with $\gamma > 0$.

Remark 1. *The aforementioned cost function and algorithm are inspired by the least-square based optimization technique with the forgetting factor in the adaptive control literature [19]. However this method is usually used to estimate an unknown constant parameter θ that takes the place of p_k in (7). Here, the problem has been generalized to the case of a time-varying parameter whose rate of change is measurable through u_k. Furthermore, compared with the gradient-based method proposed in [15], [17], we make full use of all historical data, which not only improves convergence rate, but also robustness to outliers.*

Remark 2. *A 3D implementation of algorithm (9) requires that the anchor nodes have variable heights relative to the platform, which can be unnecessarily inconvenient in most practical scenarios. To avoid this issue, we implement a 2D version of algorithm (9) in our experiment by removinng the vertical component from the distance measurement (since UWB sensor only measures the distance between two points in 3D space). More specifically, if we denote d_k^U as the distance directly measured by the UWB sensors, d_k^L as the altitude of the UAV relative to the ground as measured by some altimeter sensors, and h as the height of the platform, we can obtain $\sqrt{(d_k^U)^2 - (d_k^L - h)^2}$ as the "horizontal" distance to the anchor. This value can then be used as d_k in the calculations of algorithm (9).*

D. Exponential Convergence

In this section, we will study the exponential convergence of the relative localization algorithm under the condition that the sampling time τ is sufficiently small:

$$\tau < \frac{g(B^*)}{\sqrt{n}[U + (2N-1)a_M\Omega]},\ \hat{p}_k \in \mathbb{R}^n \tag{10}$$

where $a_M = \max_{0\le i\le N-1}\|a_i\|$, n, U and Ω are defined in Assumptions 1, 2. In the above, $g(B) = \sigma_M(B) - \sqrt{\sigma_M^2(B) - \sigma_m^2(B)}$ with $\sigma_m(B)$ and $\sigma_M(B)$ respectively denoting the smallest and the largest singular values of B, and $B^* = \arg\max_{B\in\mathcal{B}} g(B)$, where $\mathcal{B} = \{B = [b_{k_1}\dots b_{k_n}]:\ k_1\dots k_n \in \{1,2,\dots N\}\}$.

The exponential convergence theorem is stated as follows, and the proof is deferred to Appendix:

Theorem 1. *Let Assumptions 1 and 2 hold. Under condition (10), there exist $\alpha_1 > 0$ and $\alpha_2 > 0$ such that φ_k satisfies the persistent excitation (PE) condition as follows:*

$$\alpha_1 I \le \Phi(m) \triangleq \sum_{k=m}^{m+1}\varphi_k\varphi_k' \le \alpha_2 I,\ \forall m \ge 1. \tag{11}$$

As a consequence, the relative position estimate $\hat{p}_k$ will converge to the true value p_k exponentially fast under the update law (9).

IV. Experiment

In this part we will first describe our experiment setup then present and comment on the main experimental results. Note that the algorithm presented in Section III is implemented in a 2D scenario as explained in Remark 2.

A. Experiment setup

Our system is implemented on a hexacopter frame equipped with a *PX4 Autopilot*[2] flight controller computer, which also provides IMU measurements. A down-facing camera is mounted below the UAV to provide color images with a resolution of 320 × 240 pixel at 60Hz, hosted by an Intel NUC Core i7 Mini Computer. A laser range finder is used to directly measure the relative altitude (we assume that the platform's elevation from the ground is insignificant). Optical flow sensor[3] is used for velocity estimation. We refer to our previous works [18], [20] for detailed description of operation principle, advantages and limitations of UWB.

The landing platform is equipped with four UWB sensors attached to four corners of a 2m×1.5m rectangle at the same height level, one Qualcomm Snapdragon Flight board[4] attached to one of the anchor facing forward to provide VI-SLAM data, and one landing pad with markers on top. In this work, we use a visual tracking technique based on AprilTag 2 [21] with a specifically designed pattern consisting of tags with various sizes to keep the visual features within the camera's field of view (FOV) at both far and close distances, as shown in Fig. 5. As the UAV descends on the landing pad, larger tags will eventually leave the camera's FOV, while smaller ones towards the centre become detectable. Despite these considerations, we do not assume that the landing pad is always within the camera's FOV. Thus, visual position from AprilTag, UWB range measurements, and inertial data from the flight controller's IMU are fused together in the landing phase to ensure continuing relative localization and tracking for precise landing.

[2] http://px4.io
[3] https://docs.px4.io/en/sensor/px4flow.html
[4] https://developer.qualcomm.com/hardware/qualcomm-flight

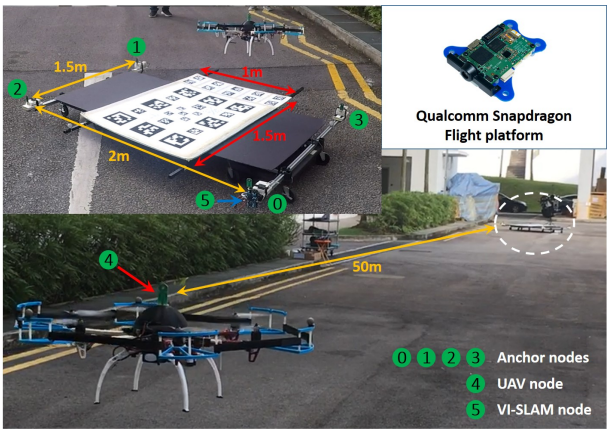

Fig. 5. Experimental setup: four anchor nodes are mounted on a flat mobile platform. The ranging sequence from the UAV node (4) is indicated by the number associated with each anchor in the figure (0-3). VI-SLAM node (5) is attached to anchor node (0), with the camera facing forward.

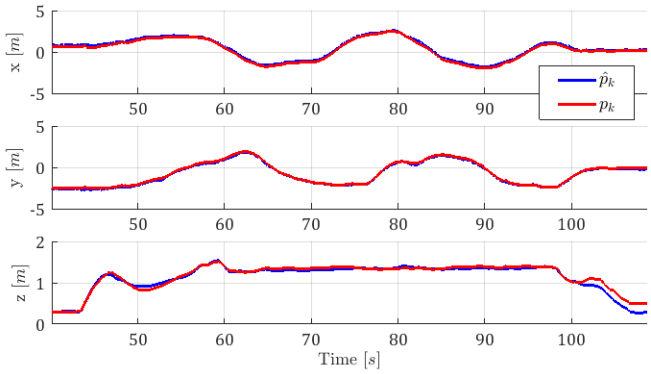

Fig. 6. Relative position estimate and ground truth in an indoor experiment (the vertical estimate is obtained directly from the laser's range finder measurement, hence we can see some small offset during the landing phase at the end due to the height of the UGV relative to the ground).

B. Results and Analysis

Three sets of experiments are carried out to investigate the performance of the system in different scenarios:

1) Static target: In the first set of experiments, a total of five flight tests were carried out in an 6m×6m indoor area with an overhead motion capture system to record the positions of the target as well as the UAV for ground truth. Due to the limited size of the testing area, we tested the algorithm with a static platform. However, in each test, we rotated the platform to a different direction before the UAV started flying. After this, the UAV was controlled manually to take off and move around the target for some time to record the relative position estimate at different directions. Then, the autonomous mode was enabled and the UAV began executing the aforementioned estimation-control schemes to approach and land on the platform.

We collected the data of all five experiment results and made some analyses. Table I shows the root mean square (rms) and standard deviation (std) values of the relative position error. Fig. 6 shows the relative position estimate together with the ground truth of one flight test. It can be seen that the average error in the position estimate is around 20 cm, which is obviously adequate for the docking operation.

TABLE I

ROOT MEAN-SQUARE (RMS) ERROR AND STANDARD DEVIATION (STD) OF RELATIVE POSITION ESTIMATES (UNIT: m).

Exp.	rms($\tilde{p}_{k,x}$)	rms($\tilde{p}_{k,y}$)	std($\tilde{p}_{k,x}$)	std($\tilde{p}_{k,y}$)
1	0.1348	0.2317	0.0956	0.1197
2	0.1677	0.1639	0.0976	0.1391
3	0.1561	0.1216	0.1198	0.0819
4	0.1717	0.0968	0.1349	0.0827
5	0.1685	0.0995	0.0619	0.0575

2) Moving target: In the second set of experiments, so called chasing experiments, five more flight tests were conducted in an outdoor environment. In these tests, the UAV took off at some distance from the target and was switched to autonomous mode to chase after the moving platform. In Fig. 7, we show the trajectories of both the target and the UAV in one of these tests. Note that p_k^M denotes the UGV's planar trajectory as measured by its visual odometry system. Thus the UAV's estimated trajectory can be visualized by adding the relative position estimate $\hat{p}_k$ to p_k^M.

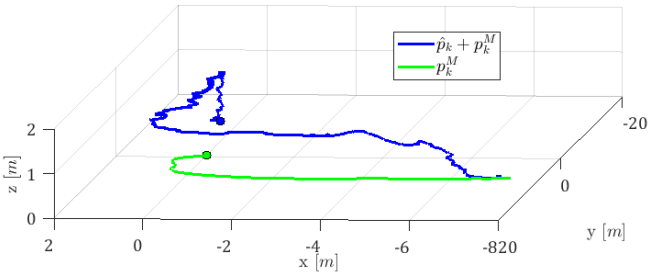

Fig. 7. Trajectories of the UAV and the target relative to the starting point of the target. The starting point of each trajectory is marked by a solid circle. A successful landing can be observed at the end of the trajectories as they coincide.

As no ground truth is available in this outdoor scenario, we use the distance measurement to represent the successful pursuit and landing on the target of the UAV. Fig. 8 shows the distance measurements to the four anchors on the target in all five tests. It can be seen that from a far distance, as the UAV successfully lands on the target, all of the distances decrease to approximately 1.25m, which corresponds to a landing spot at the center of the 2m×1.5m platform with 4 anchors at the corners.

3) Distant static target: In the final set of experiments, to validate the extent to which UAV can approach the platform, we moved the UAV to a location that is 50 m from the starting position. The platform was kept static in this case. As can be seen in Fig. 9, all of the distances still decrease to approximately 1.25 m, which verifies the capability of the UAV to approach and land on the target from about 50m away. We are confident that the method can still work at a much longer distance.

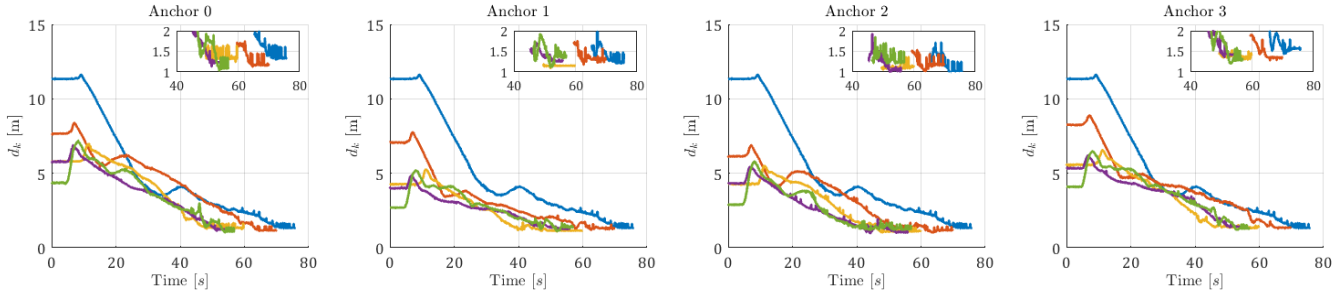

Fig. 8. Distances from the UAV to the 4 anchors as measured by UWB in the second set of experiments. From some starting position, all distances reduce to 1.25 m in the end, which reflects the successful docking task.

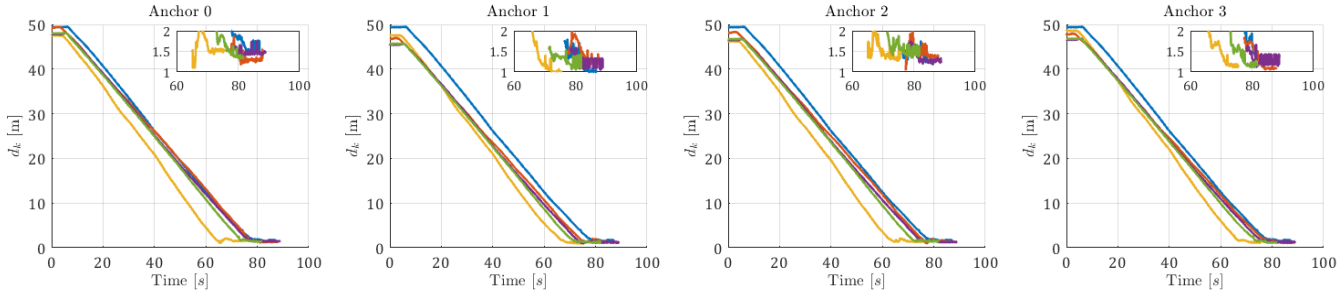

Fig. 9. Distances from the UAV to the 4 anchor as measured by UWB in the third set of experiments. From 50 m away, all distances reduce to 1.25 m in the end, which reflects the successful docking task.

V. Conclusions

In this paper we have developed a system to achieve autonomous docking capability for a quadcopter using distance and displacement measurements. Our technique complements the conventional vision-based landing techniques with a flexible relative localization scheme to allow the UAV to approach the target without the use of any external positioning information. Real-world experiments were conducted to demonstrate the efficacy of the proposed scheme.

Appendix
Proof of Theorem 1

We firstly note that $\Phi(m) = \sum_{k=m}^{m+N-1} \varphi_k \varphi_k'$ is a summation of $\varphi_k \varphi_k'$ over an interval N. Since $\varphi_k = \tau u_k - R_k a_k + R_{k-1} a_{k-1}$ and a_k takes value from a_0 to a_{N-1} periodically, it incurs no loss of generality to only show (10) for $\Phi(1)$. Below we will show $\alpha_1 I \le \Phi(1) \le \alpha_2 I$ by two steps.

1) $\Phi(1) \le \alpha_2 I$. Equivalently, we will show that there exists $\alpha_2 > 0$ such that $x'\Phi(1)x \le \alpha_2$ for any unit vector x. By recalling (6) it holds that

$$\varphi_k = R_0 b_k + c_k, k = 1, 2, \ldots, N, \tag{12}$$

where $b_k = a_k - a_{k-1}$ and $c_k = \tau u_k + (R_0 - R_k)a_k + (R_{k-1} - R_0)a_{k-1}$. By recalling Assumption 2 as well as $\|R_k a_i - R_{k-1} a_i\| \le \tau \|a_i\| |\omega_k|$ in Fig. 2, we get that

$$\begin{aligned} \|c_k\| &\le \tau U + \tau a_M N \Omega + \tau a_M (N-1)\Omega \\ &\le \tau [U + (2N-1) a_M \Omega] \triangleq c(\tau). \end{aligned} \tag{13}$$

Direct computation shows that

$$\begin{aligned} x'\Phi(1)x &\le \textstyle\sum_{k=1}^{N} (\|b_k\|^2 + 2\|c_k\|\|b_k\|^2 + \|c_k\|^2) \\ &\le N(2a_M + c(\tau))^2 \triangleq \alpha_2, \end{aligned} \tag{14}$$

where we used $\|R_0' x\| = \|x\| = 1$, (13), and $\|b_k\| \le 2a_M$, as well as the Cauchy-Swartz inequality. Thus $\Phi(1) \le \alpha_2 I$.

2) $\Phi(1) \ge \alpha_1 I$. Equivalently, we will show that there exists $\alpha_1 > 0$ such that $x'\Phi(1)x \ge \alpha_1$ for any unit vector x. Let us select $b_{k_1}, \ldots b_{k_n}$ satisfying Assumption 1, and denote $B = [b_{k_1} \ldots b_{k_n}]$. We have $\Phi(1) \ge \varphi_{k_1}\varphi_{k_1}' + \cdots + \varphi_{k_n}\varphi_{k_n}'$. Direct computation shows that

$$\begin{aligned} x'\Phi(1)x &\ge \|x' R_0 B\|^2 - 2x'CB'R_0'x + \|C'x\|^2 \\ &\ge \sigma_m^2 - 2\sigma_M \|C'x\| + \|C'x\|^2, \end{aligned} \tag{15}$$

where σ_m and σ_M are respectively the smallest and the largest singular values of B, and $C = [c_{k_1} \ldots c_{k_n}]$. Note that $\sigma_M \ge \sigma_m > 0$ by Assumption 1. Clearly, it suffices to show that $\sigma_m^2 - 2\sigma_M\|C'x\| + \|C'x\|^2 \ge \alpha_1$ for some $\alpha_1 > 0$. Noticing that $\|C'x\| \le \sqrt{n}c(\tau)$, we can see that if $\alpha_1 < \sigma_m^2$, then the above can be achieved with $c(\tau) \le (\sigma_M - \sqrt{\sigma_M^2 - \sigma_m^2})/\sqrt{n}$. Taking $B = B^*$ in (10), we have shown that $\Phi(1) \ge \alpha_1 I$.

By combing 1) and 2) we obtain the PE condition of φ_k. To study the convergence rate, let us denote $\tilde{p}_k \triangleq \hat{p}_k - p_k$ as the estimation error. By comparing (9a) and (7), we have $\epsilon_k = -\varphi_k' \tilde{p}_{k-1}$. By substituting this into (9c) and subtracting both sides by p_k, one has $\tilde{p}_k = A_k \tilde{p}_{k-1}$, where $A_k \triangleq I - \Gamma_k \varphi_k \varphi_k'$. Combining with (9b), we can prove the exponential convergence of $\tilde{p}_k$ along a similar line as in the Theorem 1 of [22].

REFERENCES

[1] A. Gautam, P. Sujit, and S. Saripalli, "A survey of autonomous landing techniques for uavs," in *Unmanned Aircraft Systems (ICUAS), 2014 International Conference on*. IEEE, 2014, pp. 1210–1218.

[2] S. Jin, J. Zhang, L. Shen, and T. Li, "On-board vision autonomous landing techniques for quadrotor: A survey," in *Control Conference (CCC), 2016 35th Chinese*. IEEE, 2016, pp. 10 284–10 289.

[3] R. Brockers, S. Susca, D. Zhu, and L. Matthies, "Fully self-contained vision-aided navigation and landing of a micro air vehicle independent from external sensor inputs," in *Unmanned Systems Technology XIV*, vol. 8387. International Society for Optics and Photonics, 2012, p. 83870Q.

[4] S. Yang, S. A. Scherer, and A. Zell, "An onboard monocular vision system for autonomous takeoff, hovering and landing of a micro aerial vehicle," *Journal of Intelligent & Robotic Systems*, pp. 1–17, 2013.

[5] M. Laiacker, K. Kondak, M. Schwarzbach, and T. Muskardin, "Vision aided automatic landing system for fixed wing uav," in *Intelligent Robots and Systems (IROS), 2013 IEEE/RSJ International Conference on*. IEEE, 2013, pp. 2971–2976.

[6] K. Ling, "Precision landing of a quadrotor uav on a moving target using low-cost sensors," Master's thesis, University of Waterloo, 2014.

[7] K. E. Wenzel, A. Masselli, and A. Zell, "Automatic take off, tracking and landing of a miniature uav on a moving carrier vehicle," *Journal of intelligent & robotic systems*, vol. 61, no. 1, pp. 221–238, 2011.

[8] D. Falanga, A. Zanchettin, A. Simovic, J. Delmerico, and D. Scaramuzza, "Vision-based autonomous quadrotor landing on a moving platform," in *IEEE/RSJ International Symposium on Safety, Security and Rescue Robotics (SSRR)*, no. EPFL-CONF-232507, 2017.

[9] A. Borowczyk, D.-T. Nguyen, A. Phu-Van Nguyen, D. Q. Nguyen, D. Saussié, and J. Le Ny, "Autonomous landing of a multirotor micro air vehicle on a high velocity ground vehicle," *IFAC-PapersOnLine*, vol. 50, no. 1, pp. 10 488–10 494, 2017.

[10] D. B. Wilson, A. Göktogan, and S. Sukkarieh, "Guidance and navigation for uav airborne docking." in *Robotics: Science and Systems*, vol. 3, no. 3, 2015.

[11] W. Kong, D. Zhang, X. Wang, Z. Xian, and J. Zhang, "Autonomous landing of an uav with a ground-based actuated infrared stereo vision system," in *Intelligent Robots and Systems (IROS), 2013 IEEE/RSJ International Conference on*. IEEE, 2013, pp. 2963–2970.

[12] Y. Gui, P. Guo, H. Zhang, Z. Lei, X. Zhou, J. Du, and Q. Yu, "Airborne vision-based navigation method for uav accuracy landing using infrared lamps," *Journal of Intelligent & Robotic Systems*, vol. 72, no. 2, p. 197, 2013.

[13] G. Loianno, C. Brunner, G. McGrath, and V. Kumar, "Estimation, control, and planning for aggressive flight with a small quadrotor with a single camera and imu," *IEEE Robotics and Automation Letters*, vol. 2, no. 2, pp. 404–411, 2017.

[14] D. Honegger, L. Meier, P. Tanskanen, and M. Pollefeys, "An open source and open hardware embedded metric optical flow cmos camera for indoor and outdoor applications," in *Robotics and Automation (ICRA), 2013 IEEE International Conference on*. IEEE, 2013, pp. 1736–1741.

[15] T.-M. Nguyen, Z. Qiu, M. Cao, T. H. Nguyen, and L. Xie, "An integrated localization-navigation scheme for distance-based docking of uavs," in *Intelligent Robots and Systems (IROS), 2018 IEEE/RSJ International Conference on*. IEEE, 2018.

[16] ——, "Single landmark distance based navigation," *Submitted to IEEE Transactions on Control Systems Technology*, 2019.

[17] T. H. Nguyen, M. Cao, T.-M. Nguyen, and L. Xie, "Post-mission autonomous return and precision landing of uav," in *2018 15th International Conference on Control, Automation, Robotics and Vision (ICARCV)*. IEEE, 2018, pp. 1747–1752.

[18] T.-M. Nguyen, A. H. Zaini, C. Wang, G. Kexin, and L. Xie, "Robust Target-relative Localization with Ultra-wideband Ranging and Communication," in *Robotics and Automation (ICRA), 2018 IEEE International Conference on*. IEEE, 2018.

[19] P. Iannou and B. Fidan, *Adaptive Control Tutorial*. Society for Industrial and Applied Mathematics: Philadelphia, PA, 2006.

[20] T. M. Nguyen, A. H. Zaini, K. Guo, and L. Xie, "An ultra-wideband-based multi-uav localization system in gps-denied environments," in *2016 International Micro Air Vehicles Conference*, 2016.

[21] J. Wang and E. Olson, "AprilTag 2: Efficient and robust fiducial detection," in *2016 IEEE/RSJ International Conference on Intelligent Robots and Systems (IROS)*. IEEE, oct 2016, pp. 4193–4198.

[22] R. M. Johnstone, C. R. Johnson, R. R. Bitmead, and B. D. Anderson, "Exponential convergence of recursive least squares with exponential forgetting factor," in *Decision and Control, 1982 21st IEEE Conference on*. IEEE, 1982, pp. 994–997.